BCS-BEC crossover and the disappearance of Fulde-Ferrell-Larkin-Ovchinnikov correlations in a spin-imbalanced one-dimensional Fermi gas

F. Heidrich-Meisner,[1,2,3] A. E. Feiguin,[4,5,6] U. Schollwöck,[1] and W. Zwerger[7]

[1]*Physics Department and Arnold Sommerfeld Center for Theoretical Physics, Ludwig-Maximilians-Universität München, D-80333 München, Germany*

[2]*Institut für Theoretische Physik C, RWTH Aachen University, D-52056 Aachen, Germany, and JARA—Fundamentals of Future Information Technology, Research Centre Jülich, D-52425 Jülich, Germany*

[3]*Kavli Institute for Theoretical Physics, University of Santa Barbara, California 93106, USA*

[4]*Department of Physics and Astronomy, University of Wyoming, Laramie, Wyoming 82071, USA*

[5]*Condensed Matter Theory Center, University of Maryland, College Park, Maryland 20742, USA*

[6]*Microsoft Project Q, University of California, Santa Barbara, California 93106, USA*

[7]*Physik Department, Technische Universität München, D-85747 Garching, Germany*

(Received 21 August 2009; published 26 February 2010)

We present a numerical study of the one-dimensional BCS-BEC crossover of a spin-imbalanced Fermi gas. The crossover is described by the Bose-Fermi resonance model in a real space representation. Our main interest is in the behavior of the pair correlations, which, in the BCS limit, are of the Fulde-Ferrell-Larkin-Ovchinnikov (FFLO) type, while in the Bose-Einstein condensate limit, a superfluid of diatomic molecules forms that exhibits quasi-condensation at zero momentum. We use the density matrix renormalization group method to compute the phase diagram as a function of the detuning of the molecular level and the polarization. As a main result, we show that FFLO-like correlations disappear well below full polarization close to the resonance. The critical polarization depends on both the detuning and the filling.

DOI: 10.1103/PhysRevA.81.023629 PACS number(s): 03.75.Ss, 71.10.Pm, 03.75.Mn, 74.20.Fg

I. INTRODUCTION

Ultracold atoms provide a unique opportunity to study basic many-body problems both in equilibrium and in nonequilibrium situations [1]. A particularly appealing feature of these systems is the possibility of changing the interaction strength over a wide range via Feshbach resonances. In a two-component Fermi gas, this allows one to study the crossover from BCS-pairing to a Bose-Einstein condensate (BEC) of strongly bound molecules [1–3]. In a situation in which the two states involved in the pairing are equally populated, this is a smooth crossover. By contrast, in the case of an imbalanced gas, unconventional superfluid ground states such as the Fulde-Ferrell [4] or Larkin-Ovchinnikov [5] (FFLO) state with finite-momentum pairs, a Sarma phase with two Fermi surfaces [6], or a mixture consisting of a BEC of strongly bound pairs and a Fermi gas of unpaired atoms have been proposed [7–11]. Experimentally, spin-imbalanced two-component Fermi gases have first been realized at MIT [12–14] and Rice [15,16]. From the spin-resolved density profiles and, in particular, the existence of a lattice of quantized vortices in a rotating gas [13], it is possible to observe the disappearance of a conventional superfluid in the center of the cloud with increasing imbalance. By assuming that a local density approximation applies, this allows one to determine the breakdown of BCS-type pairing beyond a critical imbalance p_c^{3D} that is close to $p_c^{3D} \sim 0.4$ for the uniform gas at unitarity in three dimensions [17,18].

Unfortunately, in the three-dimensional (3D) case and in the unitary regime, where the scattering length is much larger than the average interparticle spacing, it is difficult, both experimentally and theoretically, to establish unambiguously the existence of phases with unconventional pairing that are expected when the balanced ($p = 0$) superfluid becomes unstable. The experimentally observed density profiles [17] at the unitary point are consistent with the prediction of a first-order transition from a balanced superfluid to a normal state, in which the two spin components each form a Fermi liquid [2]. This theoretical prediction is based on a variational ansatz for the ground state [18,19], which excludes unconventional superfluid phases. It is therefore of considerable interest to study models, for which the phase diagram of the imbalanced gas along the BCS-BEC crossover is accessible by methods that are sensitive to states with complex order.

In the case of one dimension, such powerful numerical and analytical tools are indeed available. In fact, for both the attractive fermionic Hubbard model [20] and the associated continuum model [21,22], there is an exact solution that can be extended to the imbalanced case [23–27]. The ground-state phase diagram consists of three phases: a balanced superfluid, a polarized intermediate phase, and a fully polarized, normal Fermi gas [28]. In the weak-coupling limit, both a solution of the Bogoliubov de Gennes equations [29] and bosonization [30] indicate that the polarized intermediate phase is an FFLO-like state at any finite imbalance. This prediction has been recently verified by density matrix renormalization group (DMRG) [31–35] and quantum Monte Carlo (QMC) calculations [36,37]. It applies both to the continuum case and in the presence of an optical lattice, and the FFLO state exists in mass-imbalanced systems as well [38–41]. It is important to point out that these methods give access to the regime of strong interactions as well, where the energy scale of the superfluid states is of the same order as the Fermi energy. In the context of cold atoms, this is the relevant regime because, in weak coupling, nontrivial order only appears at unobservably low entropies of $s \simeq T_c/T_F \ll 1$ per particle.

 ©2010 The American Physical Society

As realized by both Fuchs *et al.* [42] and Tokatly [43], however, attractive fermion models are not sufficient to account for the full physics of the BCS-BEC crossover in one dimension. Indeed, in the strong-coupling limit, they describe a Tonks-Girardeau gas of dimers. They are unable, therefore, to cover the regime of weakly interacting bosons that is reached when the size of the two-particle bound state is smaller than the oscillator length of the transverse confinement. In this limit, the hard-core constraint of the tightly bound dimers becomes irrelevant. Moreover, in models of attractively interacting fermions there is only one phase at a finite spin imbalance below saturation, namely the FFLO phase [23–25,30–34,36]. As we shall emphasize in this work, the generic phase diagram of a more general two-channel model is much richer, in particular, close to resonance.

A description of the 1D BCS-BEC crossover that properly accounts for the coexistence of fermions and bound pairs in the imbalanced case can be achieved in the framework of the Bose-Fermi resonance model [44,45] in which two fermions in an open channel couple resonantly to a diatomic molecule in a closed channel. The associated amplitude due to the off-diagonal coupling between the open and closed channel determines the intrinsic width of the Feshbach resonance [1]. In a continuum description, the 1D Bose-Fermi resonance model has been studied by Recati *et al.* [46] for the special case of a vanishing imbalance, where a smooth BCS-BEC crossover occurs. Its BCS side is described by attractively interacting fermions while on the BEC side, one has a repulsive Bose gas of dimers. In the limit of a broad Feshbach resonance, the transition between the two regimes is sharp, yet continuous. In particular, the quasi-long-range superfluid order of the ground state does not change along the full BCS-BEC crossover. As realized recently by Baur *et al.* [47] in a study of the associated three-body problem, however, the situation is more complex and interesting in the case of an imbalanced gas. There, FFLO physics with spatially modulated pair correlations that are present on the BCS side of the crossover must disappear at a critical point, giving room to a Bose-Fermi mixture that is a conventional superfluid, where quasi-condensation appears at zero total momentum. At the three-body level, this critical point shows up as a change in the symmetry of the ground-state wave function [47].

For studies on the many-body physics of the 1D Bose-Fermi resonance model, we refer the reader to Refs. [46,48–51]. Bosonization has been applied to the balanced case in Refs. [48,49], and Bethe ansatz results for the imbalanced case have been presented in Refs. [50,51]. FFLO correlations, however, have not been discussed in either of these studies.

Experimentally, the formation of molecules in Fermi gases that are tightly confined in two transverse directions has been demonstrated by the ETH group [52], using a balanced mixture. The binding energy of molecules is finite for an arbitrary sign of the 3D scattering length a, in contrast to the situation without confinement, where the two-particle binding energy vanishes on the BCS side of negative a.

The objective of this work is to study a spin-imbalanced Fermi gas described by the Bose-Fermi resonance model Hamiltonian. We use a real-space representation with a finite, incommensurate filling and map out the zero-temperature phase diagram by computing pair correlations as a function of polarization and detuning. We find that FFLO correlations [4,5] dominate in a wide parameter range, and we clarify how the presence of molecules affects the stability of this phase. Qualitatively, the presence of molecules binds a certain fraction of minority fermions into molecules, reducing the overall number of pairs in the FFLO channel. As a main result, we determine the critical polarization in the crossover region at which FFLO correlations disappear and its dependence on filling and detuning. Beyond this critical polarization and below saturation, the system is a superfluid of composite bosons in the molecular channel immersed in a gas of either fully or partially polarized fermions. As a numerical tool, we employ the DMRG method [53–55].

This exposition is organized as follows. First, in Sec. II, we introduce the model Hamiltonian and discuss its limiting cases. Further, in Sec. II B, we analytically solve the two-body problem. In Sec. III, we present our DMRG results for the pair correlations, the momentum distribution, and the number of molecules as a function of filling, polarization, and detuning. We close with a summary and discussion in Sec. IV.

II. THE BOSE-FERMI RESONANCE MODEL

A. Hamiltonian

We use a minimal Hamiltonian for the 1D BCS-BEC crossover [46,47] in a real-space version, incorporating the kinetic energies of fermions and molecules, the detuning of the molecular level, as well as the coupling between the fermions and molecules:

$$H = -t\sum_{i=1}^{L-1}(c_{i,\sigma}^{\dagger}c_{i+1,\sigma} + \text{H.c.}) - t_{\text{mol}}\sum_{i=1}^{L-1}(m_i^{\dagger}m_{i+1} + \text{H.c.}) - (\nu + 3t)\sum_{i=1}^{L} m_i^{\dagger}m_i + g\sum_{i=1}^{L}(m_i^{\dagger}c_{i,\uparrow}c_{i,\downarrow} + \text{H.c.}). \quad (1)$$

$c_{i,\sigma}^{(\dagger)}$ is a fermionic annihilation (creation) operator acting on site i, while $m_i^{\dagger}$ creates a composite boson on site i. The boson energy is shifted with respect to that of single fermions by an effective detuning $\nu + 3t$. It is chosen such that the energy for adding two fermions or one boson, each at zero momentum, coincides at resonance $\nu = 0$. The amplitude for the conversion of two fermions into a closed channel molecule and vice versa is given by the Feshbach coupling constant g. For a negative detuning, $\nu < 0$, of the molecular level, it gives rise to an attractive two-particle interaction $g^2/\nu < 0$ between the fermions [46]. Near resonance, $\nu \simeq 0$, this dominates any direct background interaction U_{bg} between the two fermionic species, which is therefore neglected from the outset. The hopping matrix elements for fermions and molecules are denoted by t and t_{mol}, respectively. We further set $t_{\text{mol}} = t/2$, which accounts for the mass ratio of 2:1 between molecules and fermions. L is the number of sites. Further, $n_{i,\sigma} = c_{i,\sigma}^{\dagger}c_{i,\sigma}$, yielding the number of fermions of each species as $N_\sigma = \sum_i \langle n_{i,\sigma}\rangle$, with $N_f = N_\uparrow + N_\downarrow$ and the pseudo-spin index $\sigma = \uparrow, \downarrow$. The only conserved particle number is $N = N_f + 2N_{\text{mol}}$, where $N_{\text{mol}} = \sum_i \langle n_i^{\text{mol}}\rangle$; $n_i^{\text{mol}} = m_i^{\dagger}m_i$. We use $n = N/L$ to denote the filling factor and $p = (N_\uparrow - N_\downarrow)/N$ as a measure of the polarization, which we shall also sometimes refer to as

imbalance. Note that at maximum one molecule can sit on a single site (i.e., the molecules behave as hard-core bosons).

B. Two-body problem and spin gap

1. Scattering amplitude and bound-state energy

In this section, we calculate the effective interaction between two fermions that is mediated by the molecules at the two-body level. Following the method outlined in [46], we determine the bound-state energy $\epsilon_b > 0$ of two fermions by the condition

$$D_0^{-1}(k=0,\omega=-\epsilon_b)=\Pi(k=0,\omega=-\epsilon_b),$$

where $D_0(k,\omega)$ is the bare molecular propagator and $\Pi(k,\omega)$ is the self-energy of the closed channel propagator (with, as usual, ω and k denoting frequency and momentum, respectively).

The resulting equation

$$\epsilon_b-\nu=g^2\int_{-\pi}^{\pi}\frac{dk}{2\pi}\frac{1}{\epsilon_b+4t(1-\cos k)} \tag{2}$$

admits a unique, real solution $\epsilon_b > 0$ irrespective of the sign of the detuning ν. Of particular interest is the binding energy $\epsilon^\star=\epsilon_b(\nu=0)$ at resonance. Except for the scale $2t$ set by the bandwidth, it only depends on the dimensionless Feshbach coupling constant $g'=g/(2t)$. For small coupling strengths $g'\ll 1$, it is given by $\epsilon^\star/(2t)=g'^{4/3}/2^{2/3}$, while $\epsilon^\star/(2t)=g'$ for $g'\gg 1$. The ratio $\epsilon^\star/(2t)=1/(r^\star)^2$ is essentially the size of the bound state (in units of the lattice spacing) at resonance. In terms of this characteristic length, the condition for a broad Feshbach resonance is simply $nr^\star\ll 1$ [46]. Taking $\epsilon^\star(g')$ as a characteristic energy scale, we can write the equation for the dimensionless binding energy $\Omega=\epsilon_b/\epsilon^\star$ for an arbitrary value of the dimensionless detuning $\nu'=\nu/\epsilon^\star$ in the form

$$\nu'=-\sqrt{\frac{4+\epsilon^\star/(2t)}{\Omega[4+\Omega\epsilon^\star/(2t)]}}+\Omega, \tag{3}$$

which is easily solvable for the bound-state energy $\Omega(\nu')$ as a function of the detuning. The definition of Ω guarantees that $\Omega\equiv 1$ at resonance, irrespective of the value of the Feshbach coupling g'. In Fig. 1, we show the dependence of the binding energy $\Omega(\nu')$ on the detuning for three values of $g/t=0.1$, 0.5, and 1. As suggested by the preceding discussion, the $\Omega=\Omega(\nu')$ curve is practically independent of g'.

On the BCS side, where $\nu'\ll -1$, one obtains a very small binding energy $\sqrt{\Omega}=\sqrt{4+\epsilon^\star/(2t)}/(2|\nu'|)\ll 1$, approaching $\sqrt{\Omega}=1/|\nu'|$ for small values $g'\ll 1$ of the Feshbach coupling. In the BEC regime of strongly positive detuning, $\nu'\gg 1$, the binding energy

$$\Omega=\nu'+(g/\epsilon^\star)^2/\nu'+\cdots$$

follows the detuning, that is, the energy of the molecular state to leading order. As a result, the closed channel fraction

$$Z=\frac{\partial\epsilon_b}{\partial\nu}=1-\frac{(g/\epsilon^\star)^2}{\nu'^2}+\cdots \tag{4}$$

is close to one, as expected in the BEC limit. The dimensionless binding energy $\Omega=(r^\star/r_b)^2$ determines the size r_b of the bound state normalized to its value at resonance. For $\Omega\gg 1$, therefore, this size is much smaller than the lattice spacing unless $g'\gg 1$.

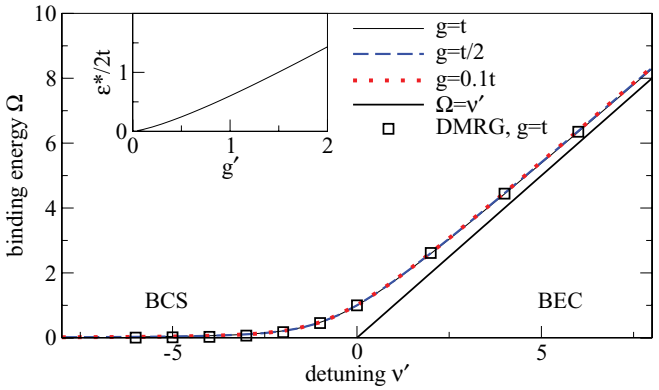

FIG. 1. (Color online) Dimensionless binding energy Ω vs detuning as computed from Eq. (3). The thick line is $\Omega=\nu'$, the asymptotic behavior in the BEC regime (see the text). For comparison, the figure includes DMRG results (squares) for the spin gap Δ at $g=t$ and a small density of $n=0.1$, extrapolated in system size to the thermodynamic limit $L\to\infty$. Inset: Characteristic energy $\epsilon^*=\epsilon(\nu'=0)$ vs g'.

2. Spin gap

In the previous section, we argued that the binding energy Ω and, in particular, ϵ^* are important quantities to characterize the 1D BCS-BEC crossover on the two-body level. We next discuss the relation of Ω to the spin gap Δ, which we calculate with DMRG as a function of filling, detuning, and the Feshbach coupling. The connection between the binding Ω and the spin gap has previously been pointed out by Orso [23].

The spin gap is computed from

$$\Delta(L)=E_0(S^z=1)-E_0(S^z=0), \tag{5}$$

where $E_0(S^z)$ is the ground-state energy of a system of length L in the subspace with $S^z=(N_\uparrow-N_\downarrow)/2$. We then extrapolate the finite-size data for $\Delta(L)$ in system size to the thermodynamic limit $L\to\infty$.

Figure 1 includes the DMRG data for the spin gap at a filling of $n=0.1$ and for $g=t$ (squares). Evidently, the spin gap coincides with the two-fermion binding energy Ω not only on the BEC side ($\nu'>1$) where this is expected, but also far into the BCS regime. Of course, for very weak coupling, this agreement must eventually be violated because the spin gap $\Delta\simeq\exp[-\pi/(2|\gamma|)]$ depends on the filling n. In particular, it is exponentially small in the dimensionless coupling constant $|\gamma|=2/(n|a_1|)\ll 1$ (where a_1 is the effective scattering length in one dimension; see [42]), while the two-particle binding energy $\epsilon_b=\epsilon^\star/\nu'^2$ is independent of n and vanishes algebraically with the detuning in this regime. Near resonance, the spin gap is identical with the two-particle binding energy in the low-density limit $nr^\star\ll 1$, as shown by Fuchs *et al.* [42]. With increasing values of the filling, however, the spin gap increases, as is evident from Fig. 2. The many-body spin gap is therefore clearly distinct from the two-particle binding energy.

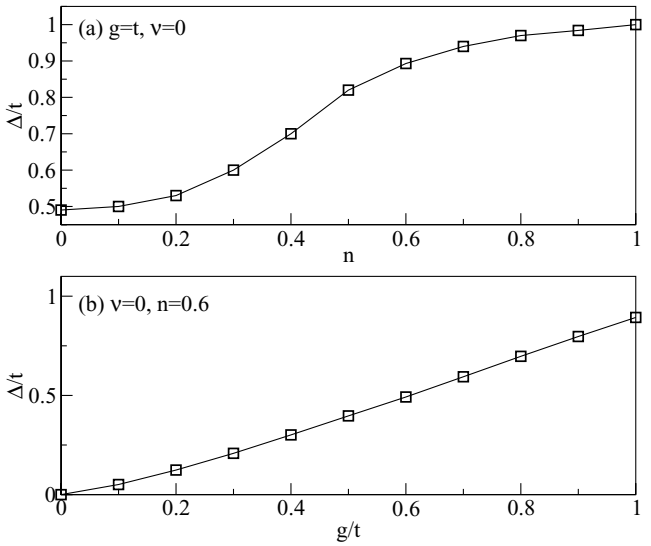

FIG. 2. Spin gap Δ at resonance $\nu = 0$ vs (a) filling n at $g = t$ and (b) Feshbach coupling g at $n = 0.6$. All results are obtained by extrapolations in system size to $L \to \infty$.

To illustrate this behavior, we display Δ as a function of filling at $g = t$ in Fig. 2(a) and as a function of g at $n = 0.6$ in Fig. 2(b), both at resonance $\nu = 0$. $\Delta = \Delta(g)$ at $n = 0.6$ also grows with the Feshbach coupling g.

C. Limiting cases of the Bose-Fermi resonance model

To guide the interpretation of our numerical results to be presented in the following sections, we find it useful to start with a qualitative discussion of the limiting cases of the Hamiltonian Eq. (1) in terms of the dimensionless detuning $\nu' = \nu/\epsilon^*$ (see also Ref. [47], which uses the more standard opposite sign convention for the detuning).

1. The BEC limit, $\nu' \gg 1$

In this limit, all particles are bound in the molecular state (i.e., $N_{\rm mol} = N/2$). At filling, $N_{\rm mol}/L < 1$, this realizes a superfluid lattice gas of hard-core bosons, that is, effectively a Tonks-Girardeau gas of molecules.

Its ground state is characterized by quasi-long-range order in the one-particle density matrix

$$\rho_{ij}^{\rm mol} = \langle m_i^\dagger m_j \rangle \tag{6}$$

in the molecular channel of the form $|\rho_{ij}^{\rm mol}| \sim x^{-1/2}$ ($x = |i - j|$) [56]. As the detuning is decreased and resonance is approached, the molecules start to make virtual fluctuations into fermions. The presence of excess fermions suppresses these fluctuations, giving rise to a repulsion between fermions and molecules which is proportional to g^2/ν [47]. Within a continuum model, this effective atom-molecule interaction on the BEC side of the resonance has been calculated exactly at the three-body level by Mora *et al.* [57]. They find that the interaction is repulsive in the regime where the two-body binding energy ϵ_b is larger by a factor 2.2 than its value $\epsilon^\star$ at resonance. For smaller binding energies, on the BCS side, the effective atom-molecule interaction becomes attractive and also nonlocal, indicating that the picture of bosons that can coexist with unpaired fermions is no longer applicable [47,57].

It is instructive to compare the regime $\nu' \gg 1$ of the lattice model studied here to the corresponding continuum model studied in Ref. [46]. In the latter case, the relevant dimensionless interaction parameter $\gamma_B = g_B/n_B$ (where n_B denotes the density of molecules) can be tuned to values small compared to one even in the deep molecular limit because $g_B \sim |\epsilon_b|^{-5/2}$ vanishes as the two-particle binding energy $|\epsilon_b|$ becomes very large. As a result, the effective Luttinger exponent $K(\gamma_B)$ is then much larger than unity and one obtains a weakly interacting gas of molecules, whose one-particle density matrix $\rho_{ij}^{\rm mol}$ decays as $|\rho_{ij}^{\rm mol}| \propto x^{-(1/2K)}$ with an exponent $1/(2K)$ that is close to zero. In the continuum and for $\nu' \gg 1$, therefore, the weakly interacting molecule gas exhibits almost true long-range order. This regime, however, is not reachable in the framework of the model given by Eq. (1), because even in the deep molecular limit ($\nu' \gg 1$), where the size of the two-particle bound state r_b (in units of the lattice spacing; see the definition of r_b given above) is much smaller than one, we still keep only the eigenvalues 0 and 1 for the local molecule occupation number $n_i^{\rm mol} = m_i^\dagger m_i$. In reality, however, more than one closed-channel molecule could sit on a lattice site in this limit because the lattice spacing is much larger than r_b. We shall not discuss or pursue this question further in the present work. Consequently, while we will be able to see the suppression of FFLO physics due to molecule formation, which is the main focus of our present work, Eq. (1) does not describe the full BCS-BEC crossover at a finite imbalance that should feature a weakly interacting BEC in the limit $\nu' \gg 1$.

2. The BCS limit, $\nu' \ll -1$

Here, $N_{\rm mol} \approx 0$. Virtual transitions into the molecular state give rise to a weak attractive on-site interaction $U = g^2/\nu$ between fermions. At a finite polarization $p > 0$, we thus expect FFLO-like correlations with real-space oscillations in the modulus of the pair-pair correlations

$$\rho_{ij}^{\rm pair} = \langle c_{i,\uparrow}^\dagger c_{i,\downarrow}^\dagger c_{j,\uparrow} c_{j,\downarrow} \rangle. \tag{7}$$

For small polarizations, these correlations are described by the sine-Gordon theory whose ground state is an array of domain walls, where the superfluid order parameter changes by π [29,30]. For larger polarizations, the domain walls merge and the order parameter acquires a purely sinusoidal form with a power-law decay

$$\left|\rho_{ij}^{\rm pair}\right| \propto |\cos(Qx)|/x^{\alpha(p)} \tag{8}$$

as a function of the separation $|i - j| = x$. The associated wave vector,

$$Q = k_{\rm F,\uparrow} - k_{\rm F,\downarrow} = \pi n p, \tag{9}$$

is fixed by the density imbalance via the difference of the Fermi wave vectors $k_{{\rm F},\sigma} = \pi N_\sigma/L$ of the majority (minority) spins. More precisely, as shown by Sachdev and Yang [58] from a generalized Luttinger theorem for Hamiltonians of the form (1), the difference $k_{\rm F,\uparrow} - k_{\rm F,\downarrow}$ of the Fermi wave vectors of the *interacting* system is quite generally fixed by the imbalance p as in Eq. (9). While the N_σ are not conserved separately in the case where the bosons are condensed, this theorem implies that the wave vector of superfluid

order in the fermions is given by Eq. (9), independently of the detuning (i.e., the strength of the interaction). In the notation of Ref. [9], the associated FFLO state is thus commensurate.

The exponent $\alpha(p)$ of the power-law decay has a quite interesting dependence on polarization and interaction strength, first discussed by Yang [30]. At vanishing polarization ($p = 0$), it is fixed by the Luttinger parameter $K_c > 1$ of the attractive 1D Fermi gas in the charge sector via $\alpha(p = 0) = 1/K_c$. In the limit of small polarizations, bosonization gives $\alpha(p > 0) = 1/K_c + 1/2$ [30], that is, a discontinuous jump of $\alpha(p)$ at $p = 0^+$. This dependence has recently been verified in Ref. [34], using the attractive 1D Hubbard model.

III. DMRG RESULTS FOR THE IMBALANCED CASE

In this section, we present our DMRG results for the number of molecules, the pair correlations, the momentum distribution function (MDF) of both fermionic components, as well as the MDF of the molecules, all as a function of polarization and detuning. As a main result we show that, while FFLO correlations are present in the BCS limit, as the number of molecules increases, the FFLO correlations disappear well below full polarization. Upon increasing the polarization at a fixed detuning and in the crossover regime, the system thus first has FFLO-like correlations, and then undergoes two phase transitions at polarizations p_1 and p_2. For $p_1 < p < p_2$, pairing at zero momentum coexists with FFLO correlations, while for $p_2 < p < 1$, the system behaves as a Bose-Fermi mixture with only one fermionic component, the majority spins. Therefore, the large-p phase is divided into a superfluid of molecules immersed in either a gas of partially polarized fermions or fully polarized fermions below saturation. We further establish that the molecular and pair correlations are identical for $p < p_1$ in the sense that they feature instabilities at the same wave vector and that their highest occupied natural orbitals are identical. Our results are summarized in phase diagrams for $g = t/2$ and $g = t$ that are presented and discussed in Sec. III C.

A. Number of molecules

To identify the crossover region characterized by a finite density of both fermions $N_f/L > 0$ and molecules $N_{\mathrm{mol}}/L > 0$, we first calculate N_{mol} as a function of the detuning ν at both $g = 0.1t$ and $g = t$. The results are depicted in Fig. 3, both for $p = 0$ and several values of the filling n [Figs. 3(a) and 3(c)] and $p > 0$ at fixed filling $n = 0.6$ [Figs. 3(b) and 3(d)].

We see that, in the balanced case, the crossover region is $-3t \lesssim \nu \lesssim t$ for $g = 0.1t$ and in the range $-4t \lesssim \nu \lesssim 4t$ for $g = t$. Moreover, the increase of N_{mol} as ν is moved from the BCS to the BEC side occurs over an increasingly wide range of detunings with increasing density n. This is consistent with the result that an abrupt change from a purely fermionic system ($N_{\mathrm{mol}} \approx 0$) to a purely molecular one ($N_f \approx 0$) only exists in the low-density limit of a broad Feshbach resonance, $nr^\star \ll 1$, as discussed previously in Refs. [42,46]. An obvious, but important consequence of the off-diagonal Feshbach coupling g is that the filling $n_f = N_f/L$ in the fermionic channel depends on the detuning and the Feshbach coupling, ranging

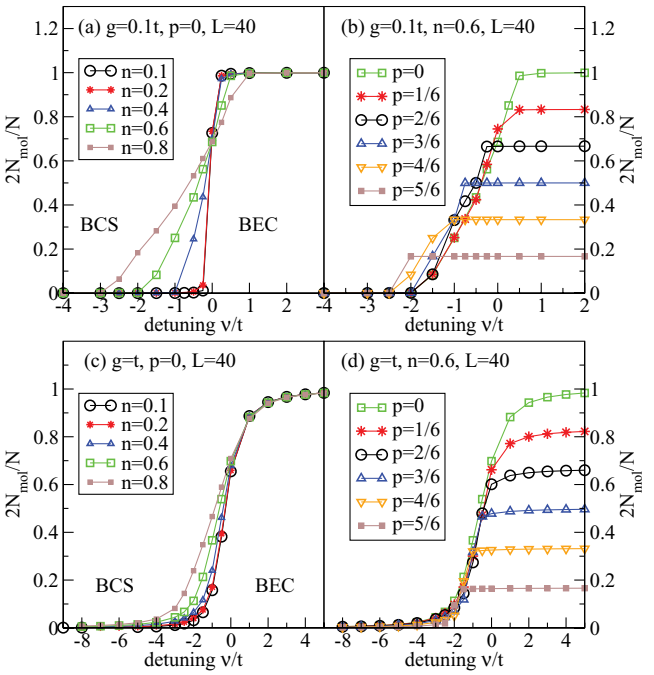

FIG. 3. (Color online) Number of molecules, N_{mol}, as a function of the detuning ν for (a, b) a resonance with $g = 0.1t$ and (c, d) a resonance with $g = t$. (a) and (c): Balanced mixture $p = 0$, with different fillings $n = 0.1$, 0.2, 0.4, 0.6, and 0.8 ($L = 40$). (b) and (d): Results for different polarizations at a filling of $n = 0.6$ ($L = 40$).

from $n_f = n$ in the $\nu' \ll -1$ limit to $n_f = 0$ in the BEC limit $\nu' \gg 1$. Therefore, the Fermi wave vectors $k_{F,\uparrow/\downarrow}$ vary, too. This is consistent with our numerical observation from Fig. 2 that the spin gap is a function of ν, n, and g.

The effect of the imbalance at some generic density n [$n = 0.6$ in Figs. 3(b) and 3(d)] is to narrow the window in which molecules and both fermionic species coexist with comparable densities. In the $g = 0.1t$ case, the detuning, at which $2N_{\mathrm{mol}} \approx N$, is shifted toward the BCS regime $\nu < 0$ as the polarization increases.

Figure 4(a) shows the number of molecules, $2N_{\mathrm{mol}}/N$, as a function of polarization and for several values of the detuning ν at $g = t$ and $n = 0.6$. As soon as the line $N_\downarrow = 0$ is reached at some polarization p_2, pairing of fermions is no longer possible, and we are left with a BEC of molecules immersed in a fully polarized gas of fermions. This sets an upper limit, well below saturation $N = N_\uparrow$, for the emergence of FFLO-like correlations. In fact, in Sec. III C, we shall see that the FFLO regime actually disappears well below p_2.

It is further instructive to compare the polarization dependence of all particle densities, that is, majority fermions $N_\uparrow/N$, minority fermions $N_\downarrow/N$, and molecules N_{mol}/N, in the crossover region and before resonance $\nu = -t$, shown in Fig. 4(b). The large-polarization region, in which $N_\downarrow/N \approx 0$, is consequently characterized by a linear dependence of N_{mol} and $N_\uparrow$ on the polarization, with the slope being independent of the detuning ν. Note that by comparing data from $L = 40$ and $L = 120$ sites, we conclude that finite-size effects are negligible for the parameters considered.

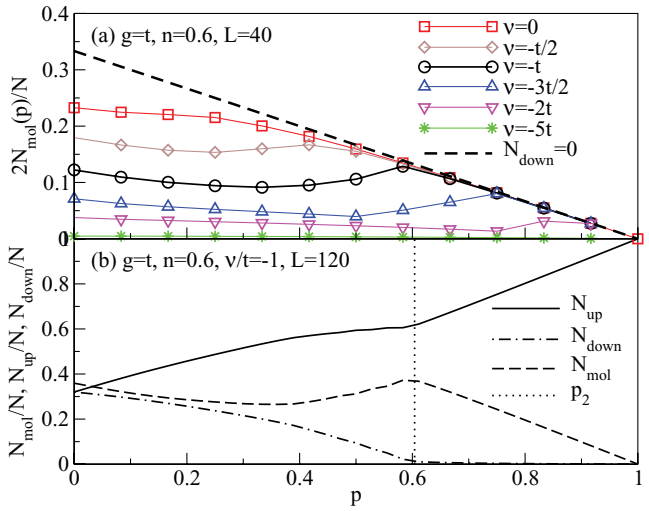

FIG. 4. (Color online) (a) Number of molecules, $N_{\rm mol}$, as a function of polarization at $n = 0.6$, $g = t$, for several values of the detuning ν. The dashed line shows the maximum possible $N_{\rm mol}$ at a given p at which $N_\downarrow = 0$. The polarization p_2 at which $N_{\rm mol}(p, \nu)$ meets that line sets an upper limit for the emergence of FFLO correlations. (b) Density of majority $N_\uparrow/N$ (solid line), minority $N_\downarrow/N$ (dot-dashed line), and molecules $2N_{\rm mol}/N$ (dashed line) as a function of polarization for $\nu = -t$ ($n = 0.6$, $L = 120$, $g = t$).

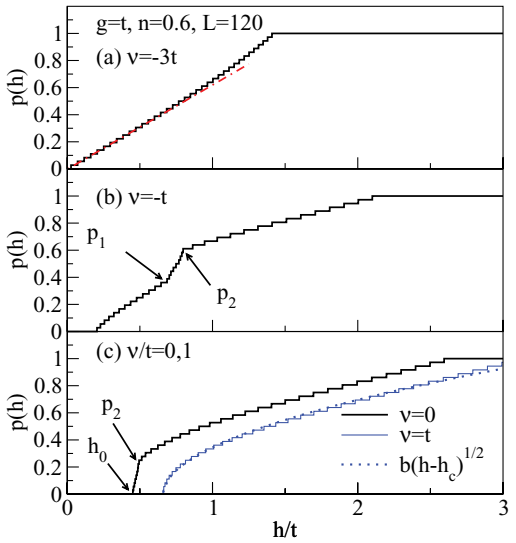

FIG. 5. (Color online) Polarization vs field h ($n = 0.6$ and $g = t$) for (a) $\nu = -3t$, (b) $\nu = -t$, and (c) $\nu = 0, t$ (thick and thin solid lines, respectively). The dash-dotted line in (a) is a fit to $p(h) = a(h - h_c)$ close to h_c, while the dotted line in (c) is a fit of the numerical data to $p(h) = b\sqrt{h - h_c}$. h_c is the critical field for the breakdown of the BEC at $p = 0$ with $N \approx 2N_{\rm mol}$.

To determine p_2, we compute the polarization curves $p = p(h)$ for a given detuning and filling n, where h denotes an effective "magnetic field," coupled to the Hamiltonian through a Zeeman-like term

$$H_{\rm field} = -h(N_\uparrow - N_\downarrow)$$

that favors a finite imbalance $p > 0$.

The results for $g = t$ and $n = 0.6$ are displayed for $\nu/t = -3$, -1, 0, and 1 in Fig. 5. For $\nu = -3t$, the $p(h)$ curve has no features and indicates the presence of a very small spin gap. At small polarization, $p = p(h)$ increases linearly with h, consistent with recent studies of the magnetization process of attractively interacting fermions [59,60]. At $\nu = -t$, we first identify the presence of a large spin gap (identified by $2h_c$) and two kink-like features at finite polarizations p_1 and p_2. Essentially, at $p > 0$, the system is a multicomponent Luttinger liquid, and the presence of kinks indicates the disappearance or appearance of one component. It is thus easy to guess that the kink at larger polarizations, p_2, is associated with the depletion of the minority fermions (i.e., $N_\downarrow \approx 0$ for $p > p_2$). This is consistent with our results for the particle densities shown in Fig. 4(b) and will be further corroborated by the discussion of the momentum distribution functions (see Sec. III B1). In view of the results for the BCS-BEC crossover of the imbalanced Fermi gas in three dimensions (see, e.g., Refs. [10,11]), one might speculate about the possibility that phase separation could appear also in one dimension. However, we stress that the critical fields h_1 and h_2 corresponding to p_1 and p_2 are well separated. In particular, a finite-size scaling analysis of the fields h_1 and h_2 for $\nu = -t$ shows that $h_2 - h_1 > 0$ remains finite in the limit of $L \to \infty$. This rules out the possibility of a jump in $p(h)$ and thus of phase separation in a uniform system.

The nature of the first kink p_1 in Fig. 5(b) will become obvious from the analysis of the pair correlations to be discussed in Sec. III B. As we shall see, below p_1, we have pairing at a finite momentum (i.e., the 1D FFLO state), molecules and the two fermionic components, while at $p > p_1$, additional pairing at zero momentum are formed. On resonance, that is, at $\nu = 0$, we still identify a kink at p_2, while on the BEC side ($\nu = t$), the polarization curve is smooth, with $p(h) \propto \sqrt{h - h_c}$, where the critical field h_c for the onset of a finite polarization $p \neq 0$ is in fact connected to the spin gap by the simple relation $2h_c = \Delta$ [23].

This behavior is characteristic for a band-filling transition of a single component, which in this case are the majority spins. Note that the same square-root dependence in magnetization curves has been found for a 1D Bose-Fermi mixture [51].

B. Pair correlations and superfluidity of molecules

1. *Momentum distribution functions for pairs, molecules, and fermions*

To address the key questions of (i) the existence of FFLO-like correlations and (ii) their stability against the presence of molecules, we compute the momentum distribution function of pairs ($n_k^{\rm pair}$) and then the momentum distribution function of the molecules ($n_k^{\rm mol}$) by taking a Fourier transformation of the real-space data for Eq. (7) and of the one-particle density matrix of the molecules, $\rho_{ij}^{\rm mol}$ [compare Eq. (6)], respectively. In the following we focus on $g = t$, unless otherwise stated.

The results for $n_k^{\rm pair}$ and $n_k^{\rm mol}$ and a filling of $n = 0.6$ are shown in Fig. 6 and Fig. 7, respectively. We choose three values of the detuning: $\nu = -3t$ [panels (a)], which is on the BCS side, $\nu = -t$ [panels (b)] in the crossover region, and finally

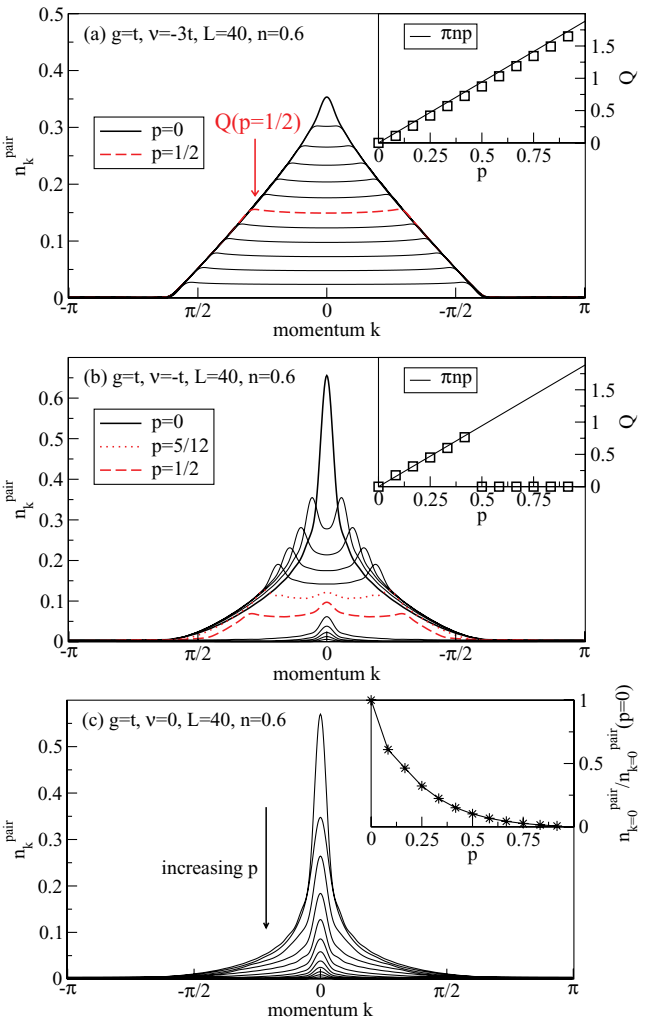

FIG. 6. (Color online) Fourier transform of pair correlations at $g = t$ and $n = 0.6$, as a function of polarization. (a) $\nu = -3t$, BCS regime; (b) $\nu = -t$, crossover region; (c) $\nu = 0$, on resonance. The insets in (a) and (b) show the position Q of the maximum in n_k^{pair} vs polarization p (squares). The solid lines in these insets are $k_{F\uparrow} - k_{F\downarrow} = \pi np$. The inset in (c) shows $n_{k=0}^{\text{pair}}$ vs polarization.

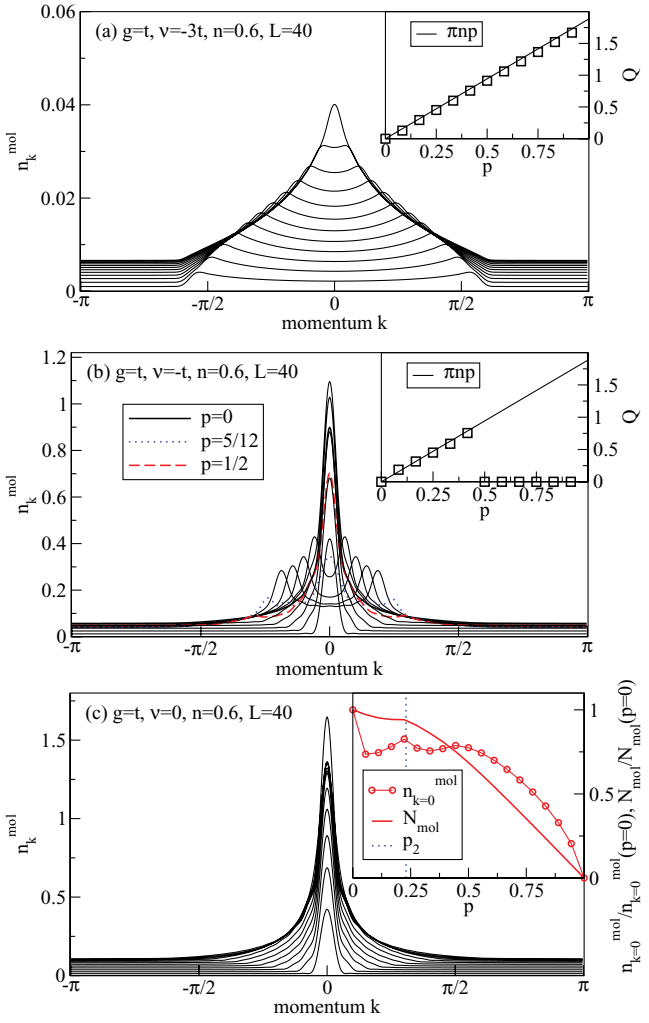

FIG. 7. (Color online) Momentum distribution of the molecules at $g = t$ and $n = 0.6$ as a function of polarization. (a) $\nu = -3t$, BCS regime; (b) $\nu = -t$, crossover region; (c) $\nu = 0$, on resonance. The insets in (a) and (b) show the position Q of the maximum in n_k^{mol} vs polarization p. In the FFLO region, the MDF of the molecules shows a peak at $Q = k_{F,\uparrow} - k_{F,\downarrow}$. The inset in (c) shows $n_{k=0}^{\text{mol}}/n_{k=0}^{\text{mol}}(p=0)$ (circles) and $N_{\text{mol}}/N_{\text{mol}}(p=0)$ vs polarization ($L = 60$).

$\nu = 0$ [panels (c)] on resonance. It is instructive to contrast the behavior of these quantities with that of the momentum distribution functions of majority and minority spins, that is, $n_k^{\uparrow,\downarrow}$, displayed in Fig. 8. n_k^{σ} is the Fourier transform of the one-particle density matrix $\rho_{ij}^{\sigma} = \langle c_{i,\sigma}^{\dagger} c_{j,\sigma} \rangle$.

Starting with the Fourier transform of pair correlations, we note that, in the BCS limit and as the polarization is increased, we observe quasi-coherence peaks at a finite momentum $Q > 0$ [see Fig. 6(a)]. Yet, these peaks are weak and the pairs' MDF resemble the one of a weakly interacting two-component Fermi gas described by the attractive Hubbard model. (Note that the finite-Q peak is more pronounced in the molecules' MDF [Fig. 7(a)]). The rather weak peaks are probably a consequence of the fact that the pair correlations differ from a pure cosine [as suggested by Eq. (8)]. This is certainly the case at small values ($p \ll 1$) of the polarization (see, e.g., Ref. [29] and the discussion in Sec. II C).

The position Q of the maximum in n_k^{pair} follows $k_{F,\uparrow} - k_{F,\downarrow}$, as we illustrate in the insets of Figs. 6(a) and 6(b). This, as usual, is a defining feature of the 1D FFLO state.

The quasi-coherence peaks are considerably more pronounced in the crossover region (i.e., $\nu = -t$), which is of primary interest in this work [see Fig. 6(b)]. We observe the breakdown of FFLO-like correlations at a finite polarization $0 < p_c^{\text{1D}} < 1$. This critical polarization p_c^{1D} is smaller than the upper limit p_2 previously discussed. An emergent feature of the pairs' MDF in the crossover region $\nu \sim -t$ is the coexistence of peaks at both $Q = 0$ and $Q > 0$ at intermediate polarization [see, e.g., the dotted line in Fig. 6(b)]. By determining the polarization at which we see pairing at both $Q = 0$ and $Q > 0$ [the dotted line in Fig. 6(b)], we find that this coincides with the first kink seen at p_1 in the polarization versus magnetic field curves shown in Fig. 5(b). Therefore, we conclude that the first phase transition and thus the boundary of the 1D FFLO phase in

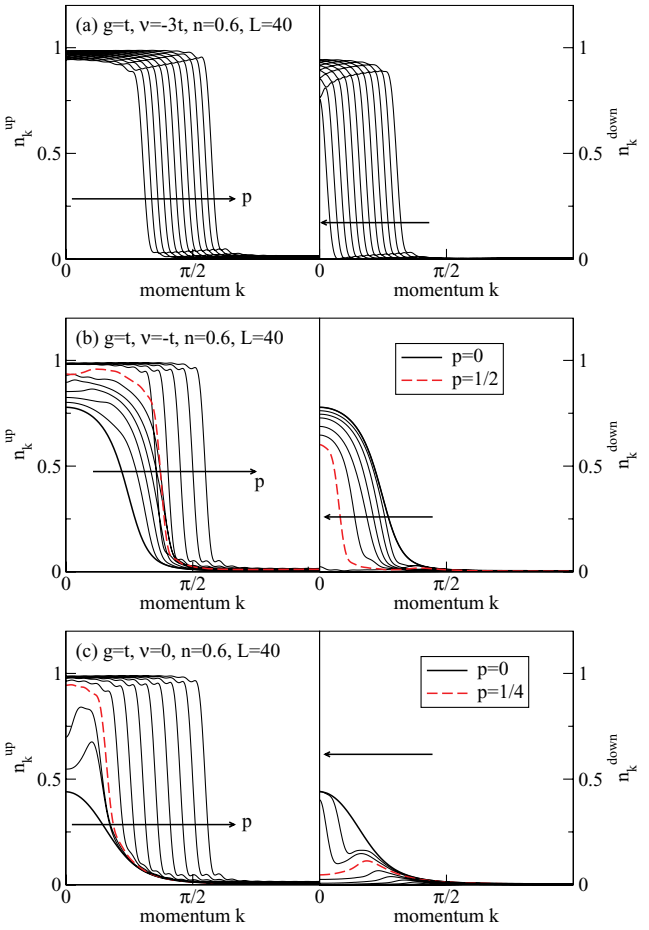

FIG. 8. (Color online) Momentum distribution functions n_k^σ at $n = 0.6$, $g = t$, as a function of polarization [left panels: $\sigma = \uparrow$; right panels: $\sigma = \downarrow$]. (a) $\nu = -3t$, BCS regime; (b) $\nu = -t$, crossover region; (c) $\nu = 0$, on resonance. Arrows indicate increasing polarization p. In the case of panel (b), $n_k^\downarrow \approx 0$ for $p > 1/2$.

the crossover regime and at $p > 0$ is the one at $p = p_1$ where pairing at $Q = 0$ starts to contribute, effectively adding an additional quasi-long-range order parameter to the system. We can further define a crossover polarization $p^* > p_1$, beyond which the dominant instability is at $Q = 0$. In the example of $\nu = -t$ shown in Fig. 6(b), $p^* = 1/2$. Note that slightly above p^*, some modulation in the pairs' MDF survives, which shows up as a smaller maximum in n_k^{pair} at a finite momentum. Finally, we note that the FFLO correlations are typically enhanced at low densities (e.g., at $n = 0.2$; results not shown here). To summarize, we identify p_c^{1D} with the upper boundary of the FFLO phase (i.e., $p_c^{\text{1D}} = p_1$).

Right at resonance ($\nu = 0$), signatures of FFLO correlations are no longer visible, and the momentum distribution functions of both the pairs and the molecules feature a maximum at zero momentum [see Figs. 6(c) and 7(c)]. We observe the same behavior on the BEC side, $\nu > 0$. For illustration, the $k = 0$ weight in the pair and molecular MDFs are shown as a function of polarization in the insets of Figs. 6(c) and 7(c). Quite notably, $n_{k=0}^{\text{mol}}$ exhibits features that can be related to the phase transitions the system undergoes as p increases. First, the weight discontinuously drops from its $p = 0$ value, as the critical field for breaking up molecules is overcome at $p = 0^+$. Second, $n_{k=0}^{\text{mol}}$ takes a maximum at p_2, where the system enters into the Bose-Fermi mixture phase at $p > p_2$. A similar, yet less significant behavior can be seen in the number of molecules, $N_{\text{mol}}(p)/N_{\text{mol}}(p = 0)$, which we have included in the inset of Fig. 7(c) for comparison (solid line) [see also Fig. 4(b)].

An important point that should be emphasized in this context is the fact that the respective quasi-condensates of molecules and fermions are locked into each other. Indeed, they qualitatively show the same behavior concerning the position of their maxima, as is evident from comparing Figs. 6 and 7.

We next discuss the MDF of the two fermion components, shown in Fig. 8. In the BCS limit, the MDFs feature a sharp edge, reminiscent of a weakly interacting lattice gas and consistent with the features observed in Fig. 6(a). As ν moves the system into the BEC regime, the $p = 0$ MDFs become quite broad, as expected for a strongly interacting system and for the standard BCS-BEC crossover (see, e.g., Refs. [1,61]). Upon polarizing the system, $n_k^\uparrow$ develops a sharper edge [see Figs. 8(a), 8(b), and 8(c), left panels], as eventually only the majority fermions remain. This is particularly evident in the case of $\nu = -t$ shown in Fig. 8(b): For $p > 1/2$, $N_\downarrow = \sum_k n_k^\downarrow \approx 0$. Simultaneously, for $p > 1/2$, $n_k^\uparrow$ changes from a smooth function seen at $p \leqslant 1/2$ to a steep one, since for $p > 1/2$, there is a single fermionic component left. Thus the depletion of minority fermions characterizes the transition to the Bose-Fermi mixture phase at $p \geqslant p_2$.

2. *Natural orbitals*

To render the analysis of the locking effect [46,48,49,62] between ρ_{ij}^{pair} and ρ_{ij}^{mol} more quantitative, we compute the eigenvalues and eigenvectors (sometimes called "natural orbitals") of the associated one-particle density matrices, ρ_{ij}^{pair} and ρ_{ij}^{mol}. In particular, the orbital ϕ_0 that is connected with the largest eigenvalue according to the Penrose-Onsager decomposition [63] of the density matrix reveals the real-space structure of the quasi-condensates [64]. In the presence of FFLO-type order, ϕ_0 is therefore a nontrivial function even for a homogeneous system. The modulus of this quantity, that is, $|\phi_0|$, is plotted in Fig. 9(a) for $n = 0.2$ and in Fig. 9(b) for $n = 0.6$, in both cases for $p = 0, 1/6$ and values of the detuning such that the system is in the crossover regime.

Both at $p = 0$ and in the FFLO phase, the natural orbitals of molecules and pairs are fully identical, as has been shown for the limit of vanishing polarization in previous studies [46,49]. Further, in the 1D FFLO phase, the spin density

$$\langle S_i^z \rangle = (\langle n_{i,\uparrow} \rangle - \langle n_{i,\downarrow} \rangle)/2$$

follows the real-space modulation of the natural orbital, with excess majority fermions residing in the nodes of the quasi-condensate (compare Refs. [29,31] for the case of the 1D attractive Hubbard model). In contrast to the behavior of the spin density, the density of molecules follows the modulation of the quasi-condensate. In other words, the molecular density has its maxima and minima at the same positions as the natural orbital. We should stress here that the presence of features in the densities are due to the open boundary conditions used in our simulations. In the limit of $L \to \infty$, the density and spin profiles will become flat, while the modulations

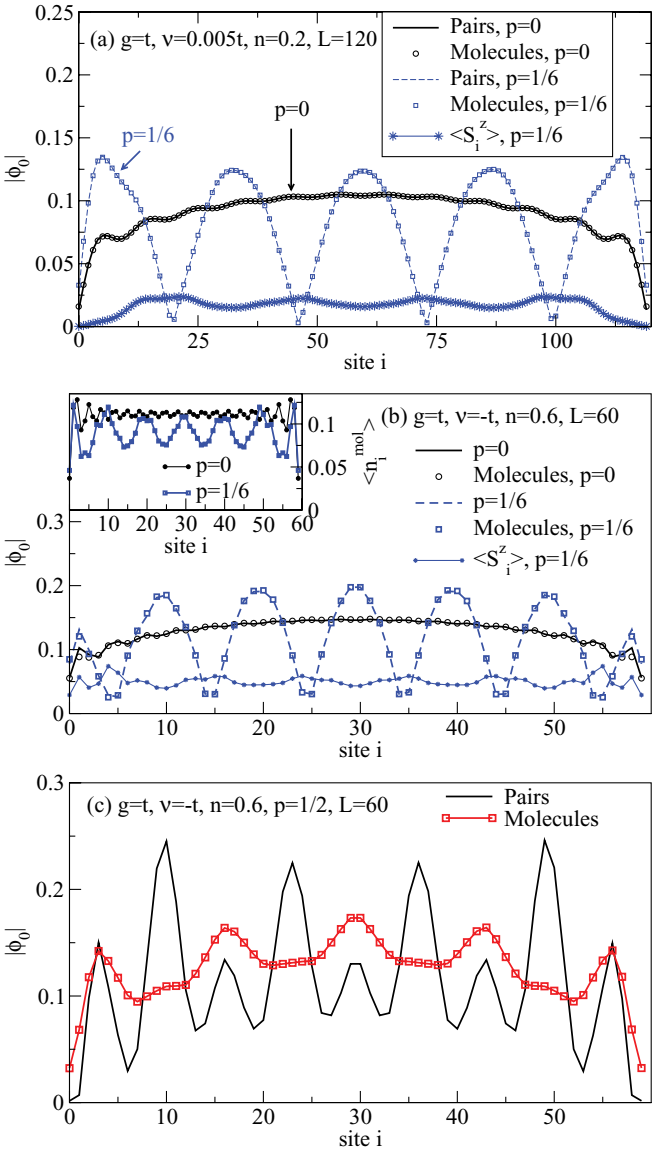

FIG. 9. (Color online) Natural orbital $|\phi_0|$ for pairs (lines) and molecules (symbols) for (a) $n = 0.2$, $\nu = 0.005t$ and (b) $n = 0.6$, $\nu = -t$, both at $p = 0, 1/6$ (circles and squares, respectively). The stars are $\langle S_i^z \rangle$ for $p = 1/6$. The inset in (b) shows the density of molecules $\langle n_i^{\mathrm{mol}} \rangle$ at $p = 0, 1/6$. (c) Natural orbitals in the intermediate phase $p_1 < p < p_2$ for $\nu = -t$, $p = 1/2$, $g = t$, and $L = 60$.

can then be detected in the respective correlation functions (compare Refs. [33,65] for the attractive Hubbard model). In the experimentally relevant situation of harmonically trapped particles, however, the density profiles themselves should have properties similar to those discussed here for finite systems with open boundary conditions, at least in parts of the particle cloud.

Note that, in the regime $p_1 < p < p_2$, the molecular and the pair correlations still exhibit instabilities at the same wave vectors [see Fig. 9(c)], even though the natural orbitals differ in their amplitude. The locking effect (i.e., natural orbitals of pairs and molecules with the same amplitude) is re-encountered in the high-field region $p_2 < p < 1$. There, the molecular $|\phi_0|$ is

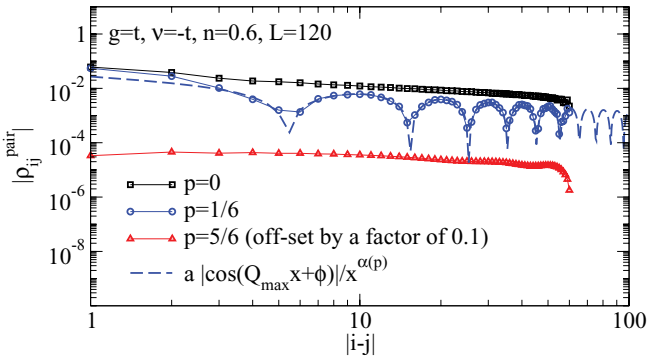

FIG. 10. (Color online) Decay of pair correlations in real space for $g = t$, $n = 0.6$, $\nu = -t$, and $p = 0, 1/6, 5/6$. Symbols denote DMRG results from $L = 120$ sites while the dashed line is a fit of $f(x) = a|\cos(Qx + \phi)|/x^{\alpha(p)}$ [30] to the numerical data. The fit parameters are a, α, and ϕ, while Q is taken from the Fourier transform of the pair correlations. The $p = 5/6$ curve is offset by a factor of 0.1 for clarity.

smooth, while the corresponding natural orbital for the pairs exhibits small oscillations.

3. *Spatial decay of pair correlations*

To conclude our analysis of the pair correlations, we show that the pair correlations at $n = 0.6$ asymptotically decay as $|\rho_{ij}^{\mathrm{pair}}| \propto |\cos(Qx)|/x^{\alpha}$, $x = |i - j|$, in agreement with predictions from bosonization for the slowest decaying contribution to $|\rho_{ij}^{\mathrm{pair}}|$ [30]. To that end, we fit

$$f(x) = a|\cos(Qx + \phi)|/x^{\alpha}$$

to our numerical data, measuring j away from the center of the system (i.e., $i = L/2$). Given that the system sizes are not that large, the agreement between the DMRG results and the formula from bosonization is remarkable [see Fig. 10]. In the regime, where FFLO correlations have completely disappeared, the pair correlations decay with a power law, as Fig. 10 suggests for the example of $p = 5/6$. Small oscillations are due to an inhomogeneous background density of pairs and molecules [compare the inset of Fig. 9(b)].

Finally, we have also verified that, at $p = 0$ and in the BEC limit $\nu' \gg 1$, our numerical data are consistent with a power-law decay of the one-particle density matrix of the molecules

$$\left|\rho_{ij}^{\mathrm{mol}}\right| \propto 1/x^{\beta}$$

with an exponent of $\beta \approx 1/2$.

C. Phase diagram

Our results for the phase diagram of the 1D BCS-BEC crossover described by Eq. (1) are summarized in Fig. 11, for the cases of $g = t$ [Fig. 11(a)] and $g = t/2$ [Fig. 11(b)]. The main panels contain the data for $n = 0.6$ and we present polarization p versus dimensionless ν' detuning phase diagrams.

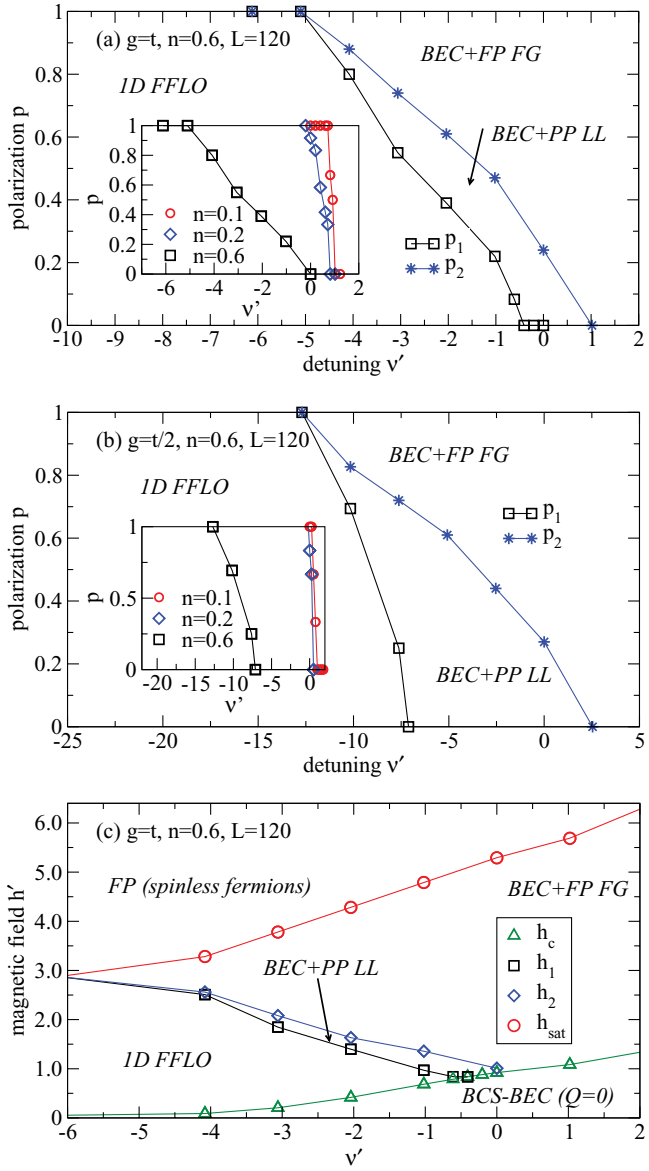

FIG. 11. (Color online) Phase diagrams of polarization p vs dimensionless detuning ν' for $n = 0.6$ and (a) $g = t$ and (b) $g = t/2$. The line $p = p_1(\nu')$ (squares) separates 1D FFLO from the *BEC + PP LL* regime. The stars denote p_2 (see Sec. III A), separating *BEC + PP LL* from *BEC + FP FG*. Insets in (a) and (b) show the dependence of p_1 on filling: $n = 0.6$ (squares), $n = 0.2$ (diamonds), and $n = 0.1$ (circles). (c) The same as in (a), yet here plotted as a magnetic field h' vs detuning ν' phase diagram. h_c (triangles) is the critical field for the breakdown of the balanced gas, while $h_{\rm sat}$ (circles) is the saturation field. Lines are guides to the eye.

We identify three regions at $p > 0$:

(i) The BEC limit, $\nu' \gg 1$ and $p_2 < p < 1$: Here, molecules are immersed in a sea of fully polarized fermions. This phase is denoted as *BEC + FP FG* in the figures, where *FP FG* stands for fully polarized Fermi gas.

(ii) The 1D FFLO phase at $0 < p < p_1$: In the crossover regime, FFLO is suppressed as p is increased. We have determined the phase boundary p_1 (open squares) from both the position of the first kink in the polarization curves and from the pair correlations. In the latter case, at p_1, the peak at $Q = 0$ starts to build up in the MDF of the pairs. For instance, the 1D FFLO phase extends up to $\nu \lesssim -0.3t$ at this filling and $g = t$. This is slightly before resonance on the BCS side, where, nevertheless, the density of molecules is already finite, that is, $N_{\rm mol} > 0$ (compare Fig. 3).

(iii) $p_1(n, \nu) < p < p_2$, beyond which we have a $Q = 0$ superfluid of molecules immersed in a partially polarized (PP) fermionic gas: This third phase, denoted by *BEC + PP LL*, is eventually replaced by the *BEC + FP FG* phase at $p \geqslant p_2$, where we determine p_2 from the analysis of $p = p(h)$ curves (see Sec. III A).

Note that the boundary of the 1D FFLO phase, p_1, depends on the filling n. From the insets of Figs. 11(a) and 11(b), we infer that the larger n, the wider the crossover region is, consistent with the discussion of the number of molecules (compare Sec. III B1). As $n \to 0$, the critical line $p = p_1$ becomes quite steep and approaches $\nu \approx (0.048 \pm 0.002)t$, or $\nu' \approx 0.97$, for $g = t$.

The comparison of the $g = t$ and the $g = t/2$ phase diagram shows that the FFLO phase disappears much faster in the case of $g = t/2$, well before resonance. Qualitatively, one can ascribe this to the fact that with decreasing values of the Feshbach coupling the number of molecules, or more precisely, the closed channel fraction [compare Eq. (4)] becomes larger. The presence of molecules tends to reduce the number of pairs with FFLO correlations. This can be expected to more efficiently suppress FFLO physics for smaller g since the locking of molecules and pairs is then also weaker. These observations are consistent with our DMRG results for the number of molecules and their dependence on polarization and detuning presented in Fig. 3. In particular, the maximum number of molecules is reached at smaller values of ν for larger polarization.

Figure 11(c) shows the data of Fig. 11(a) in the magnetic field versus detuning plane, using the dimensionless detuning ν' and field $h' = h/\epsilon^*$. This yields additional information on the saturation field $h_{\rm sat}$ and the zero-field spin gap Δ of the standard 1D BCS-BEC crossover of the balanced system, measured by h_c. In comparison with Fig. 1, where we have shown $\Delta \simeq \epsilon^*$ for $n = 0.1$, we repeat that the spin gap $\Delta = 2h_c$ is an increasing function of the filling n [compare also Fig. 2(a)]. In the limit of $\nu' \gg 1$, $\Delta = 2h_c$ behaves as $\Delta \propto \nu'$ since there, independently of filling, the ground state of the balanced system has $N \approx 2N_{\rm mol}$ and $N_f \approx 0$.

In a previous work on the three-body problem in the continuum limit, Baur *et al.* [47] have shown that the change in correlations between an oscillating behavior on the BCS side due to FFLO physics to a smooth one on the BEC is revealed in the symmetry of the three-body ground-state wave function. The numerical value of the detuning where this change occurs is $\nu'_c \approx 0.63$ [47]. It is remarkable that a similar critical value for the disappearance of FFLO correlations is also found in our many-body calculation of the phase diagram. Indeed, in the low-density limit, where a comparison makes sense, the boundary of the 1D FFLO at small polarizations is typically close to resonance, yet on the BEC side of positive detuning

$\nu > 0$. For a quantitative comparison, we have determined the critical value $\nu_c'(n = 0.1)$ for the loss of FFLO correlations for several values of g from data taken with $L = 120$ sites and polarization $p = 1/6$, the smallest imbalance possible for this system size. The resulting values are in the range of $0.55 \lesssim \nu_c' \lesssim 0.91$, remarkably close to the value inferred from three-body physics in Ref. [47].

In conclusion, it is evident from Fig. 11 that the best regime for observing the 1D FFLO state is (i) low density and (ii) small polarizations. The low density will favor a large weight in the quasi-coherence peaks, while the polarization needs to be kept smaller than p_1. Moreover, the 1D FFLO phase is more stable at large Feshbach couplings g.

IV. SUMMARY AND DISCUSSION

In this work, we studied the Bose-Fermi resonance model in the imbalanced case as a simple model to describe the BCS-BEC crossover of a spin-imbalanced system in one dimension. Our main focus was on the existence and stability of the 1D FFLO phase. So far, many-body calculations of 1D FFLO physics were mostly concerned with models of attractively interacting fermions, which do not account for the existence of composite molecules in the closed channel, typically encountered in experiments. Using a numerically exact method, the density matrix renormalization group method, we computed several quantities to characterize the crossover, including the number of molecules, pair correlations, the momentum distribution function, as well as polarization curves. Most notably, we found that FFLO correlations are suppressed in the crossover region due to the presence of the diatomic molecules. In particular, the 1D FFLO phase gives room for a regime of molecules, quasi-condensed at zero momentum. The latter is first immersed in partially polarized fermions, which is then replaced by a Bose-Fermi mixture with spinless fermions below saturation. Thus, the system undergoes two phase transitions in the crossover region at critical polarizations $p_1 < p_2 < 1$ as the polarization increases.

While our work was concerned with the homogeneous system, in experiments, the particles typically experience a confining harmonic potential. The shell structure for attractively interacting fermion models in one dimension was intensely discussed. The emerging picture for the continuum case, based on numerically or analytically exact approaches (the latter typically combined with the local density approximation) [23,24,37], is that one finds either fully paired wings at small polarization or fully polarized wings, while the core is always partially polarized. In the case of lattice models, DMRG calculations that take the trap into account exactly report fully polarized wings with a partially polarized core [31,32] at intermediate and large polarizations, and the latter also remains true in coupled chains at sufficiently large polarizations [66].

While we expect the behavior of trapped, attractively interacting fermions to carry over to the BCS regime of the Bose-Fermi resonance model, a finite density of molecules may lead to qualitatively different shell structures. For instance, the heavier molecules should mostly reside in the center of the trap. On the one hand, one may expect this to destabilize the FFLO phase in the core, while on the other hand, as long as the Feshbach coupling g and hence the locking between pairs and molecules is sufficiently strong, the locking could protect the FFLO correlations. The clarification of the effect of a harmonic trap is left for future research.

An important question is how the FFLO state can be detected in an experiment. Several proposals have been put forward, for instance, time-of-flight measurements [67], the analysis of noise correlations [34,68], or features in the spin density and correlations [65]. Regarding the spin correlations, one expects a peak at nonzero momentum $2Q \neq 0$ in the presence of FFLO order [65]. In fact, the spin density follows the modulation of the natural orbitals, as has previously been demonstrated for the 1D attractive Hubbard model [31]. As we showed here, this behavior is also realized in the FFLO phase of the Bose-Fermi-resonance model (compare Fig. 9). Even if the FFLO phase was present in a 3D system, the obstacle there would be that the FFLO phase is in the wings of a 3D, trapped Fermi gas (see, e.g., Ref. [69]). This constitutes another advantage of searching for FFLO physics in a 1D system: There, the core of a trapped gas will host this phase [23,31,37], and therefore the associated modulation in the spin density should exist in a large part of the cloud, in contrast to the 3D case.

Note added in proof. Recently, we became aware of a related, very recent experiment at Rice that studies the spin-imbalanced Fermi gas with attractive interactions in one dimension [70].

ACKNOWLEDGMENTS

We acknowledge fruitful discussions with A. Kolezhuk and we thank D. Huse and the authors of Ref. [47] for their comments on a previous version of this work. We thank E. Dagotto for granting us computing time at his group's facilities at the University of Tennessee at Knoxville. U.S. and W.Z. acknowledge support from the Deutsche Forschungsgemeinschaft through FOR 801. U.S. was further supported by the DFG through Grant No. SCHO-621/8-2. F.H.-M. thanks the KITP at UCSB for its hospitality, where part of this research was carried out. This research was supported in part by the National Science Foundation under Grant No. NSF PHY05-51164.

[1] I. Bloch, J. Dalibard, and W. Zwerger, Rev. Mod. Phys. **80**, 885 (2008).

[2] S. Giorgini, L. P. Pitaevskii, and S. Stringari, Rev. Mod. Phys. **80**, 1215 (2008).

[3] W. Ketterle and M. Zwierlein, in *Ultracold Fermi Gases, Proceedings of the International School of Physics "Enrico Fermi," Course CLXIV, Varenna, 20–30 June 2006*, edited by M. Inguscio, W. Ketterle, and C. Salomon (IOS Press, Amsterdam, 2008).

[4] P. Fulde and A. Ferrell, Phys. Rev. **135**, A550 (1964).

[5] A. Larkin and Y. Ovchinnikov, Zh. Eksp. Teor. Fiz. **47**, 1136 (1964) [Sov. Phys. JETP **20**, 762 (1965)].

[6] G. Sarma, Phys. Chem. Solids **24**, 1029 (1963).

[7] D. T. Son and M. A. Stephanov, Phys. Rev. A **74**, 013614 (2006).

[8] K. Yang and S. Sachdev, Phys. Rev. Lett. **96**, 187001 (2006).
[9] M. M. Parish, S. K. Baur, E. J. Mueller, and D. A. Huse, Phys. Rev. Lett. **99**, 250403 (2007).
[10] D. E. Sheehy and L. Radzihovsky, Ann. Phys. (NY) **322**, 1790 (2007).
[11] K. B. Gubbels, M. W. J. Romans, and H. T. C. Stoof, Phys. Rev. Lett. **97**, 210402 (2006).
[12] M. W. Zwierlein, C. H. Schunck, A. Schirotzek, and W. Ketterle, Nature (London) **442**, 54 (2006).
[13] M. W. Zwierlein, A. Schirotzek, C. H. Schunck, and W. Ketterle, Science **311**, 492 (2006).
[14] Y. Shin, M. W. Zwierlein, C. H. Schunck, A. Schirotzek, and W. Ketterle, Phys. Rev. Lett. **97**, 030401 (2006).
[15] G. B. Partridge, W. Li, R. I. Kamar, Y. A. Liao, and R. G. Hulet, Science **311**, 503 (2006).
[16] G. B. Partridge, W. Li, Y. A. Liao, R. G. Hulet, M. Haque, and H. T. C. Stoof, Phys. Rev. Lett. **97**, 190407 (2006).
[17] Y. Shin, C. H. Schunck, A. Schirotzek, and W. Ketterle, Nature (London) **451**, 689 (2008).
[18] C. Lobo, A. Recati, S. Giorgini, and S. Stringari, Phys. Rev. Lett. **97**, 200403 (2006).
[19] S. Pilati and S. Giorgini, Phys. Rev. Lett. **100**, 030401 (2008).
[20] E. H. Lieb and F. Y. Wu, Phys. Rev. Lett. **20**, 1445 (1968).
[21] M. M. Gaudin, Phys. Lett. **A24**, 55 (1967).
[22] C. N. Yang, Phys. Rev. Lett. **19**, 1312 (1967).
[23] G. Orso, Phys. Rev. Lett. **98**, 070402 (2007).
[24] H. Hu, X.-J. Liu, and P. D. Drummond, Phys. Rev. Lett. **98**, 070403 (2007).
[25] E. Zhao and W. V. Liu, Phys. Rev. A **78**, 063605 (2008).
[26] P. Kakashvili and C. J. Bolech, Phys. Rev. A **79**, 041603(R) (2009).
[27] F. Woynarovich and K. Penc, Z. Phys. B **85**, 269 (1991).
[28] F. Essler, H. Frahm, F. Göhmann, A. Klümper, and V. E. Korepin, *The One-dimensional Hubbard Model* (Cambridge University Press, Cambridge, 2005).
[29] K. Machida and H. Nakanishi, Phys. Rev. B **30**, 122 (1984).
[30] K. Yang, Phys. Rev. B **63**, 140511(R) (2001).
[31] A. E. Feiguin and F. Heidrich-Meisner, Phys. Rev. B **76**, 220508(R) (2007).
[32] M. Tezuka and M. Ueda, Phys. Rev. Lett. **100**, 110403 (2008).
[33] M. Rizzi, M. Polini, M. A. Cazalilla, M. R. Bakhtiari, M. P. Tosi, and R. Fazio, Phys. Rev. B **77**, 245105 (2008).
[34] A. Lüscher, R. M. Noack, and A. M. Läuchli, Phys. Rev. A **78**, 013637 (2008).
[35] A. E. Feiguin and D. A. Huse, Phys. Rev. B **79**, 100507(R) (2009).
[36] G. G. Batrouni, M. H. Huntley, V. G. Rousseau, and R. T. Scalettar, Phys. Rev. Lett. **100**, 116405 (2008).
[37] M. Casula, D. M. Ceperley, and E. J. Mueller, Phys. Rev. A **78**, 033607 (2008).
[38] G. G. Batrouni, M. J. Wolak, F. Hebert, and V. G. Rousseau, EPL **86**, 47006 (2009).
[39] B. Wang, Han-Dong Chen, and S. Das Sharma, Phys. Rev. A **79**, 051604(R) (2009).
[40] E. Burovski, G. Orso, and T. Jolicoeur, Phys. Rev. Lett. **103**, 215301 (2009).
[41] G. Orso, E. Burovski, and T. Jolicoeur, Phys. Rev. Lett. **104**, 065301 (2010).
[42] J. N. Fuchs, A. Recati, and W. Zwerger, Phys. Rev. Lett. **93**, 090408 (2004).
[43] I. V. Tokatly, Phys. Rev. Lett. **93**, 090405 (2004).
[44] M. Holland, S. J. J. M. F. Kokkelmans, M. L. Chiofalo, and R. Walser, Phys. Rev. Lett. **87**, 120406 (2001).
[45] E. Timmermans, K. Furuyab, P. W. Milonnia, and A. K. Kermanc, Phys. Lett. **A285**, 228 (2001).
[46] A. Recati, J. N. Fuchs, and W. Zwerger, Phys. Rev. A **71**, 033630 (2005).
[47] S. K. Baur, J. Shumway, and E. J. Mueller, e-print arXiv:0902.4653 (unpublished).
[48] E. Orignac and R. Citro, Phys. Rev. A **73**, 063611 (2006).
[49] R. Citro and E. Orignac, Phys. Rev. Lett. **95**, 130402 (2005).
[50] M. T. Batchelor, M. Bortz, X. W. Guan, and N. Oelkers, Phys. Rev. A **72**, 061603(R) (2005).
[51] X.-W. Guan, M. T. Batchelor, and J.-Y. Lee, Phys. Rev. A **78**, 023621 (2008).
[52] H. Moritz, T. Stöferle, K. Günter, M. Köhl, and T. Esslinger, Phys. Rev. Lett. **94**, 210401 (2005).
[53] S. R. White, Phys. Rev. Lett. **69**, 2863 (1992).
[54] S. R. White, Phys. Rev. B **48**, 10345 (1993).
[55] U. Schollwöck, Rev. Mod. Phys. **77**, 259 (2005).
[56] B. M. Coy, Phys. Rev. **173**, 531 (1968).
[57] C. Mora, R. Egger, A. O. Gogolin, and A. Komnik, Phys. Rev. Lett. **93**, 170403 (2004).
[58] S. Sachdev and K. Yang, Phys. Rev. B **73**, 174504 (2006).
[59] J. He, A. Foerster, X. W. Guan, and M. T. Batchelor, New J. Phys. **11**, 073009 (2009).
[60] T. Vekua, S. Matveenkov, and G. Shlyapnikov, JETP Lett. **90**, 289 (2009).
[61] T. Giamarchi, *Quantum Physics in One Dimension* (Clarendon, Oxford, 2004).
[62] D. E. Sheehy and L. Radzihovsky, Phys. Rev. Lett. **96**, 060401 (2006).
[63] O. Penrose and L. Onsager, Phys. Rev. **104**, 576 (1956).
[64] The absence of true long-range order in one dimension even at zero temperature implies that the largest eigenvalue of the one-particle density matrix does not scale linearly with particle number N or system size. Instead, it behaves like $N^{1-1/(2K)}$, where $K > 1$ is the associated Luttinger parameter.
[65] T. Roscilde, M. Rodriguez, K. Eckert, O. Romero-Isart, M. Lewenstein, E. Polzik, and A. Sanpera, New J. Phys. **11**, 055041 (2009).
[66] A. E. Feiguin and F. Heidrich-Meisner, Phys. Rev. Lett. **102**, 076403 (2009).
[67] K. Yang, Phys. Rev. Lett. **95**, 218903 (2005).
[68] T. Paananen, T. K. Koponen, P. Torma, and J.-P. Martikainen, Phys. Rev. A **77**, 053602 (2008).
[69] T. N. De Silva and E. J. Mueller, Phys. Rev. A **73**, 051602(R) (2006).
[70] Yean-an Liao, A. S. C. Rittner, T. Paprotta, Wenhui Li, G. B. Partridge, R. G. Hulet, S. K. Baur, and E. J. Mueller, e-print arXiv:0912.0092 (unpublished).